*Research Article*

# Automatic Extraction of Rock Discontinuities from the Point Cloud Using Dynamic DBSCAN Algorithm

**Ming Tang,[1] Song Yang,[1] Guohua Huang,[1] Xiongyao Xie,[2,3] Jiafu Guo,[1] and Junli Zhai [ID] [2,3]**

[1]*Powerchina Roadbridge Group CO., LTD, Beijing 100000, China*
[2]*Key Laboratory of Geotechnical & Underground Engineering of Ministry of Education, Tongji University, Shanghai 200092, China*
[3]*Zhejiang Scientific Research Institute of Transport, Hangzhou, 311305, China*

Correspondence should be addressed to Junli Zhai; 707043292@qq.com

Detection and mapping of rock discontinuities are important during excavation. The terrestrial laser scanning (TSL) technology is widely used to acquire accurate quantitative. However, there is rarely study about the influence of discontinuities parameters on the detection. Through the 3D printing technology, we have built discontinuity models with different roughness and connectors with different angles. Therefore, we can control the variables in the scanning. Several open-source packages were applied to derive the information from the point cloud acquired by TSL. The result shows that the recognition effect decreases with the angle between discontinuities. Moreover, the presence of roughness of discontinuity makes it prone to lead to lousy classification in the detection process. The proposed method has successfully extracted discontinuity dip, dip direction, and roughness automatically from the point cloud. The application on the two datasets showed great adaptability and accuracy. Consequently, the method could meet realistic engineering needs.

## 1. Introduction

Detection and mapping of rock discontinuities are important during excavation. The intersections between discontinuities, known as faults, joints, and bedding planes, divide a body of rock into fragments that detach from the larger body of rock when revealed by tunnel construction. Therefore, acquiring accurate quantitative discontinuity data, which are not affected by biases and censoring, is critical. The field mapping and handheld direct measuring with a scan-line method or a scan-window method require direct access to the excavation face. Consequently, collecting geological information on rock discontinuities is difficult, time-consuming, and often dangerous, especially in unstable areas.

Recently, the applications in geosciences of remote sensing investigations for the investigation of rock mass have rapidly improved. The most common techniques used to generate highly detailed 3D point clouds are terrestrial laser scanning and digital photogrammetry [1–5]. Several approaches have been used to construct the 3D point clouds of rock surface to obtain Digital Outcrop Model (DOM) about the excavation face. The DOM formed by these dense point clouds allows engineers to perform the information extraction on a computer. Many researchers have been working on automatically extracting discontinuity parameters (e.g., orientation, spacing, trace persistence, and roughness) from the DOM. Assali et al. [6] developed a semiautomatic process that classifies rock discontinuities into subsets according to their orientation. Chen et al. [7] presented a new method for extracting discontinuity orientation automatically from rock mass surface 3D point cloud. Chen et al. [8] discussed the accuracy of the 3D laser scanning technique and demonstrated the potential of 3D laser scanning techniques to replace traditional window mapping. Idrees and Pradhan [9] investigated the influence of rock geostructure on cave channel development. They assessed the cave's stability by determining areas susceptible

to different failure types using surface discontinuity data extracted from laser scanning point cloud. Li et al. [10] presented an automatic characterization method for rock mass discontinuities that uses 3D point clouds. The orientation, trace, spacing, roughness, and aperture are extracted automatically by this method. Monsalve et al. [11] generated the DFNs by characterizing discontinuities in an underground limestone mine by laser scan.

Unfortunately, there are some intractable technical bottlenecks. First, these studies mainly cluster the point cloud through statistical analyses of the geometric features of triangular mesh units in a TIN generated from the point clouds. However, this method only considers the small-scale local features of point cloud data. Consequently, the automatic clustering process is prone to make mistakes by uneven rock mass surfaces. Second, these approaches are mainly based on the k-means algorithm. It means that the clustering is sensitive to the selection of initial centers and the number of clusters. Third, the resample process was widely used in these methods to get uniform point clouds. Consequently, the information on the discontinuities could be varied and dismissed.

This paper proposed a novel method to extract rock discontinuities from unstructured raw point clouds automatically. Our key innovation is to achieve the goal of point cloud classification without resampling and the TIN process. The remainder of this paper is organized as follows. In Section 2, we summarize proposed methods for LiDAR point cloud classification. In Section 3, we experiment to verify the performance of our method. In Section 4, the case study was carried out. Finally, the paper is discussed and concluded in Sections 5 and 6.

## 2. Methodology

In this section, we introduce the proposed algorithm for extracting rock discontinuities from point clouds. Section 2.1 describes the random forest algorithm as a classifier for point clouds. In Section 2.2, the dynamic DBSCAN algorithm is presented.

### 2.1. Random Forest Algorithm.
RF [12] is always found to be the highest performing classifier for point clouds. RF is natively a multi-class algorithm, meaning that a single run of the model could predict all class labels. The output class probability scores represent the proportion of trees that voted for each class, and the sum of all probabilities is equal to 1 by definition. The RF classifier we trained was used to classify the point clouds into discontinuities and edges. Consequently, the input features we used in this study are the geometry features at multiple scales. The main idea behind these features is to characterize the local dimensionality properties of the scene at each point with different scales. The discontinuity looks like a 3D at a few millimeter-scale because of the roughness, and the edge also looks like a 3D object. Consequently, it is challenging to distinguish them. At a larger scale (i.e., 10 cm), the edge still looks like a 3D. By contrast, the discontinuity now looks more 2D than

3D. When combining geometry information from different scales, we can thus build signatures that identify the discontinuity and edge. Consequently, the eigenvalues of the covariance matrix of the neighborhood point $X$, $Y$, and $Z$ coordinates, searched with different scales, are calculated and sorted from largest to smallest. The eigenvalues $\lambda_1^{r_j}, \lambda_2^{r_j}, \lambda_3^{r_j}$ ($\lambda_1^{r_j} > \lambda_2^{r_j} > \lambda_3^{r_j}$) are then normalized as equation (1).

$$p_i^j = \frac{\lambda_i^{r_j}}{\lambda_1^{r_j} + \lambda_2^{r_j} + \lambda_3^{r_j}} \ (i = 1, 2, 3). \tag{1}$$

The $j$ indicates the scale of the scene. These proportions characterize the degree to which the point neighborhood can be considered 1-D, 2-D, or 3-D. These three proportions are calculated for each of the nine scene scales for 27 geometry features.

### 2.2. Dynamic DBSCAN Algorithm.
DBSCAN [13] can find several clusters with irregular shapes based on the estimated density distribution as one of the developed density-based clustering algorithms. It does not need to know the number of clusters in advance. The methodology of the traditional DBSCAN algorithm is illustrated as shown in the left part of Figure 1. Starting from a random unvisited point A, DBSCAN retrieves all points in the neighborhood with a user-defined radius $\epsilon$. The density threshold *MinPts* is the minimum number of points required to form a dense region. If at least *MinPts* points are within the $\epsilon$-neighborhood, point A would be regarded as a core point. And all its neighborhoods would be arranged into the density-reachable set. Then an unvisited point in this set will be visited randomly, and the above procedure will be repeated. If the number of $\epsilon$-neighborhood is less than Minpts, like point B, the point will be regarded as a border point. The loop will be carried on until there is no point unvisited in the density-reachable set. The other points, like point C, which is density-unreachable, should be allocated into another cluster or noise.

However, in the TSL points cloud, the density of points is anisotropic and inhomogeneous so that the hyper-parameters *MinPts* and $\epsilon$ can hardly be determined reasonably. The dynamic DBSCAN algorithm is proposed in this paper to address this shortage, as shown in the right part of Figure 2. The number of $\epsilon$-neighbor points of every point is treated as a constant *MinPts*. Moreover, the radius $\epsilon$ is a variable according to the density rather than a constant in the traditional DBSCAN algorithm.

After the border points are distinguished, the search operation shown in Figure 2 will be carried out following these steps: first, the original point $P_i$ will be selected from the points cloud set $R$ by chance. If the $P_i$ is not a border point, its $\epsilon$-neighbor points will be retrieved from $R$ into set Q. Otherwise, the operation should be suspended and the first step repeated. Then the points in set $Q$ will be visited and operated the same way as $P_i$ until there is no unvisited point in Q. The points in set $Q$ come from the same discontinuity. Finally, the points in set $Q$ will be removed from the $R$, and
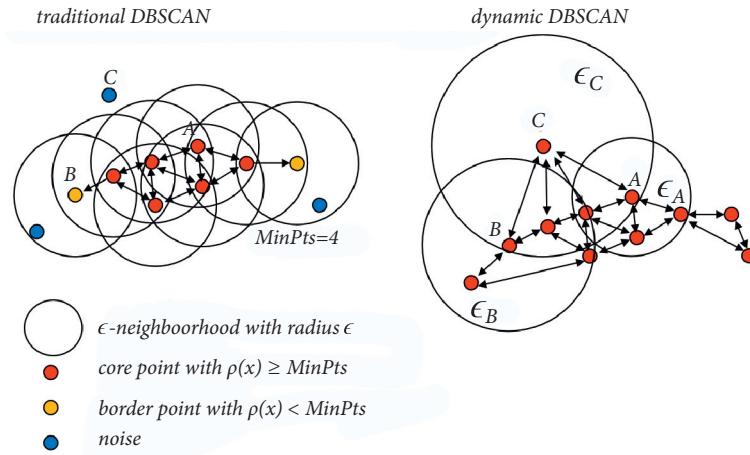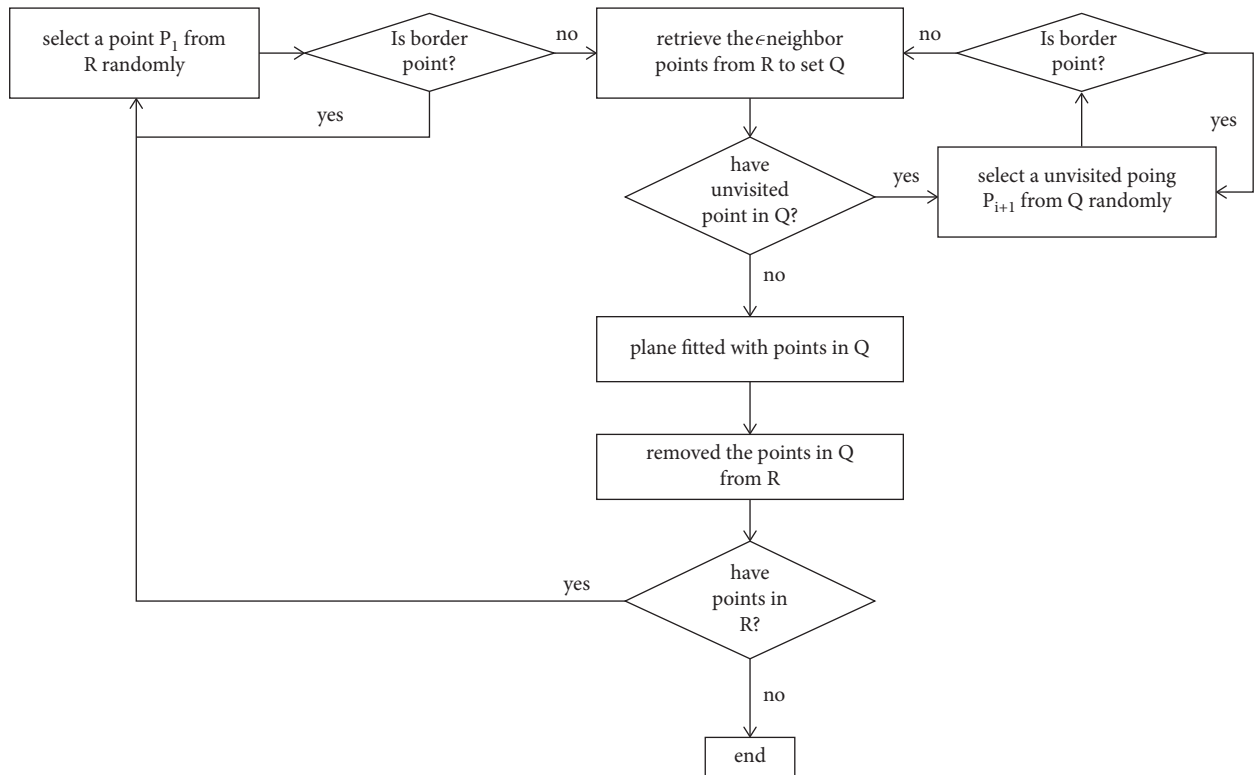
FIGURE 1: The dynamic DBSCAN algorithm.



FIGURE 2: The workflow of discontinuities clustering.

the first step will be executed repeatedly until the $R$ is empty. As shown in Figure 3, the points retrieved with the dynamic DBSCAN method from point clouds in an application are recognized as rough surfaces. Its oration will be calculated by the best plane fitted algorithm with these points instead of by the facet generated from a triangular mesh. So, the pseudosurface caused by the small-scale roughness can be avoided rationally.

## 3. Experiment

This section scans discontinuities with different roughness and angles by a laser scanner to learn how the accuracy is affected. First, the model and data preparations are described. Then, the influence of various levels of roughness and angles is shown.

*3.1. Model Design and Data Collection.* As shown in Figure 4, to investigate the influence of roughness and included angle, we design a series of plates with different roughness surfaces and connectors with different included angles. The models were scanned with a Leica C10 terrestrial laser scanner (Figure 3(b)). The scanner was positioned at 1 m to the models and operated at the highest possible angular resolution. The resulting point cloud contained about 1.2 million points on the model surface with a point-spacing of 1 mm on
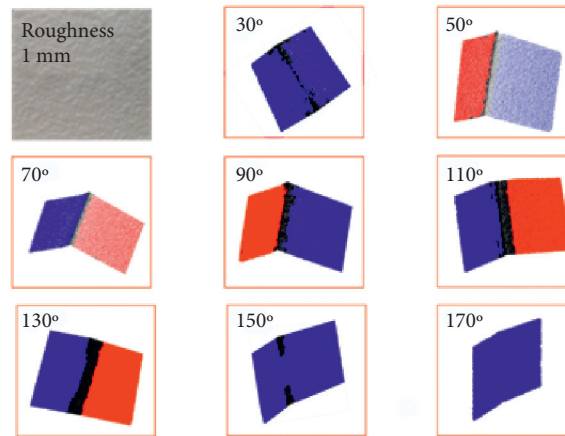
FIGURE 3: The segmentation results of discontinuities.



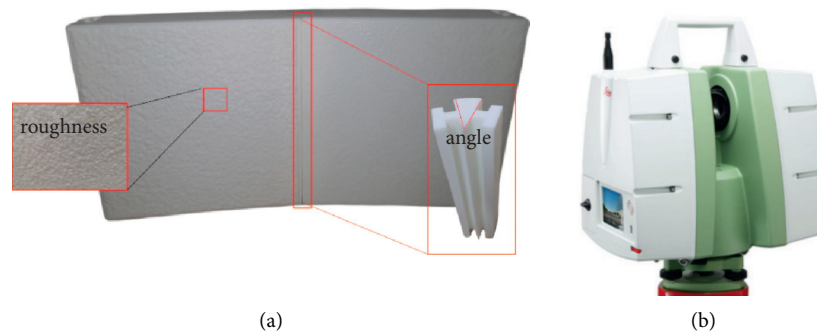(a)                                                      (b)

FIGURE 4: The experiment design.

average. According to the technical. Since the model is placed on the desk, a random rotation was carried out to get a random model.

## 4. Result and Analysis

*4.1. Classification Result.* Figure 5 is the classification result of the test point cloud, and it can be seen that the overall classification accuracy can be stabilized at about 97.3%. Table 1 is the recall of the decomposition line under the conditions of different surface roughness and different included angles. When the roughness of the discontinuity is less than 5 mm, and the included angle is less than 130°, the classifier can achieve a 100% recognition effect on the boundary. With the increase of angle and roughness of the structural plane, the classification accuracy gradually decreases. With the increase of the angle, the three-dimensional feature of the point cloud at the junction line gradually decreases, and it shows a 2D feature at each scale, so it is classified into the discontinuity category. When the roughness is large, the point cloud of discontinuity presents three-dimensional features in the multiscale field. The classifier divides the point cloud of discontinuity into the boundary category.

*4.2. Segmentation Result.* Figure 6 shows the segmentation effect of discontinuities by the DBSCAN algorithm under the conditions of 0.5 mm and 1 mm roughness of discontinuities. The black point cloud data are the identified

decomposition line points. When the included angle of the structural plane is 170°, the two discontinuities are considered as a single surface. Consequently, the segmentation of the discontinuities cannot be realized.

Figure 3 shows the segmentation effect of discontinuities under the condition of 5 mm roughness. It can be seen that when the included angle of the structural plane reaches 150°, the segmentation cannot be realized. Furthermore, when the included angle is equal to 30°, the segmentation still fails, although the boundary between the discontinuities is identified. This is because when the included angle of the discontinuities is slight, and the roughness of the discontinuities is large, the distance between the two discontinuities near the boundary is relatively close. Therefore, the DBSCAN algorithm is prone to cross between different discontinuities point clouds when searching the neighbors, leading to the error.

## 5. Case Study

The application in two cases is introduced in this section. Case A consists of regular polygons scanned in laboratory conditions; case B is points from a portion of a rock slop, available at http://www.3D-landslide.com/projects/discontinuity/.

*5.1. Case A.* As shown in Figure 7, two representative geometric shapes, cube, and dodecahedron, were selected for analysis. The cube is represented using 60,488 points, and the
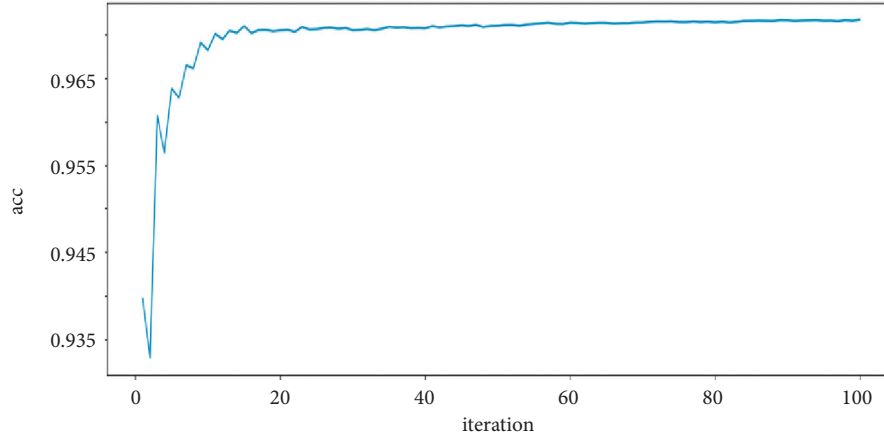
FIGURE 5: The RF learning curve.

TABLE.1: The recall in classification.

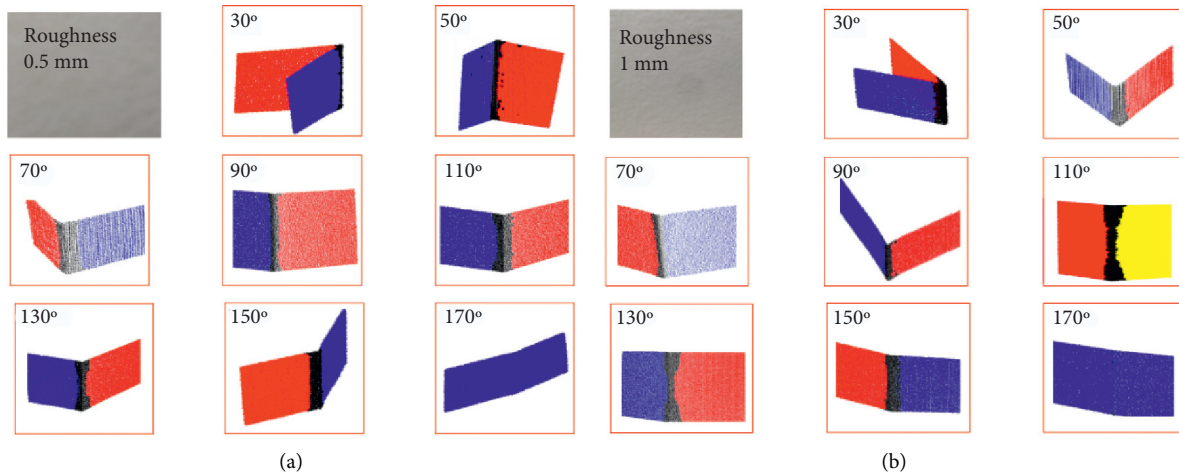| Roughness (mm) | Angle | | | | | | | |
|---|---|---|---|---|---|---|---|---|
| | 30° | 50° | 70° | 90° | 110° | 130° | 150° | 170° |
| 0.5 | 1 | 1 | 1 | 1 | 1 | 0.98 | 0.84 | 0.66 |
| 1 | 1 | 1 | 1 | 1 | 1 | 0.99 | 0.72 | 0.61 |
| 5 | 1 | 0.97 | 0.97 | 0.99 | 0.95 | 0.96 | 0.55 | 0.51 |



(a) (b)

FIGURE 6: The segmentation results of discontinuities.

dodecahedron is represented using 80,828 points. Data were obtained using a 3D digitizer (Konica Minolta, Vivid 9i) through progressive rotation of the objects around a fixed platform axis and subsequent scanning.

Figure 8 shows the result of the automatic grouping of the cube and dodecahedron point clouds. The cube can be grouped into five different discontinuities, and the dodecahedron can be grouped into six different discontinuities. Different colors represent each discontinuity. The Silhouette validity index (SVI) is calculated to evaluate the validity of the clustering as follows.

$$S(x_i) = \frac{b(x_i) - a(x_i)}{\max\{a(x_i), b(x_i)\}}. \tag{2}$$

The $x_i$ is a sample in one of the clusters. $a(x_i)$ is defined as the average distance of $x_i$ to all other samples in its cluster, and $b(x_i)$ is defined as the minimum of the average distance between $x_i$ and samples in other clusters. A S(xi) value close to 1 indicates that $x_i$ is assigned to an appropriate cluster. If $S(x_i)$ is close to -1, xi is misclassified and lies somewhere between the clusters. The average SVI is all data points in the whole dataset. The SVI is shown in Figure 8 and compared with reference [6].

The Silhouette values corresponding to different methods are shown in Figure 8. The hollow mark presented the results from reference [6]. As the number of clusters must define manually, the maximum SVI corresponds to three and six for the cube and the dodecahedron. However,
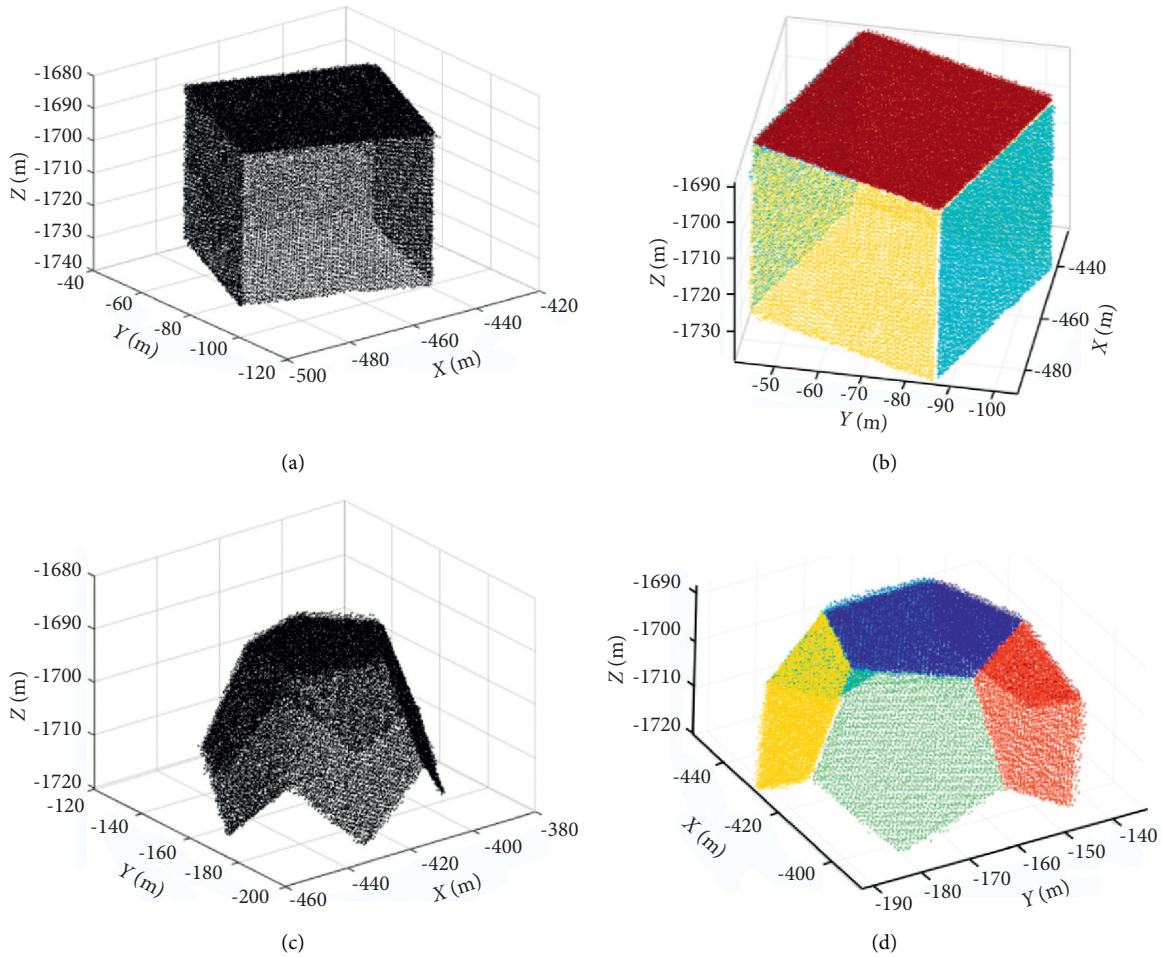
(a)



(b)



(c)



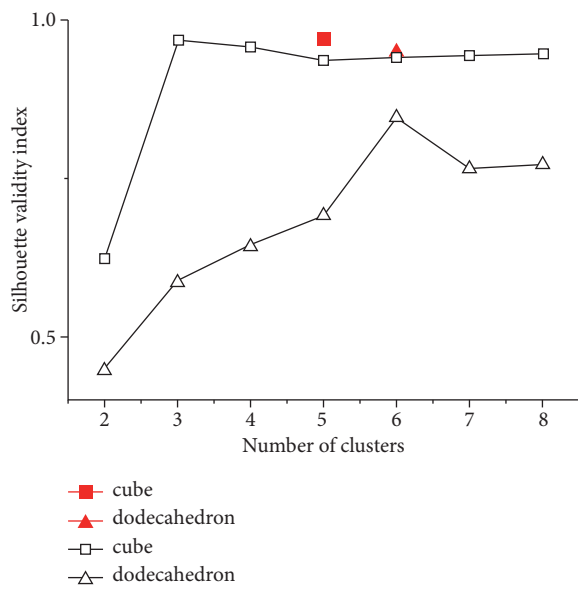(d)

FIGURE 7: Automatic clustering analysis results.



FIGURE 8: SVI compared with reference [6] in different numbers of clusters. The solid marks depict the results of the dynamic DBSCAN algorithm, and the hollow marks present the result from the reference [6].

the preknowledge in the number of clusters could be ignored in the dynamic DBSCAN algorithm. Furthermore, in our method, the SVI, presented by the red solid mark, is better than that in reference [6].

*5.2. Case B.* As shown in Figure 9, case B was a portion of a rock slope, which covers an area of approximately $6\,\mathrm{m^2}$ with an average point spacing of 0.0055 m. After classifying points to discontinuities, the RANSAC plane fitting algorithm considers the volatility and produces an objective estimate of the discontinuity orientations. Details of the RANSAC method have been introduced in reference [8]. Figure 9(b) shows the result of the automatic grouping of the discontinuities.

$$dip = \frac{180 \times \arctan\sqrt{A^2 + B^2}/|C|}{\pi},$$

$$dip - direction = 180 \times \arctan|B/A|/\pi. \tag{3}$$

The dip and dip direction statistics are represented in Figure 10. The discontinuities could be divided into five groups according to the density distribution characteristics
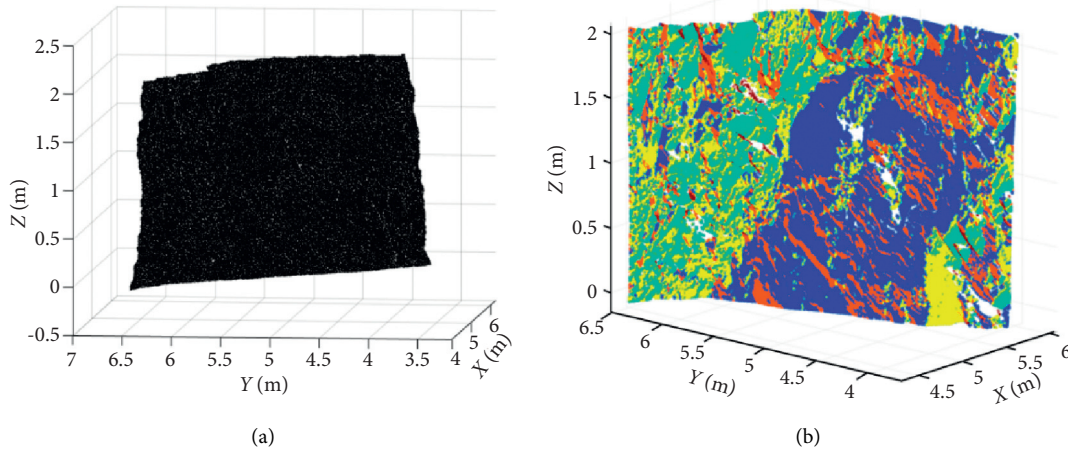
(a)

(b)

FIGURE 9: Automatic clustering results. Consequently, the discontinuity plane parameters could be obtained. Furthermore, assuming the plane equation is $Ax + By + C(z) + D = 0$, the discontinuity dip and dip direction could be recovered with equation (3).
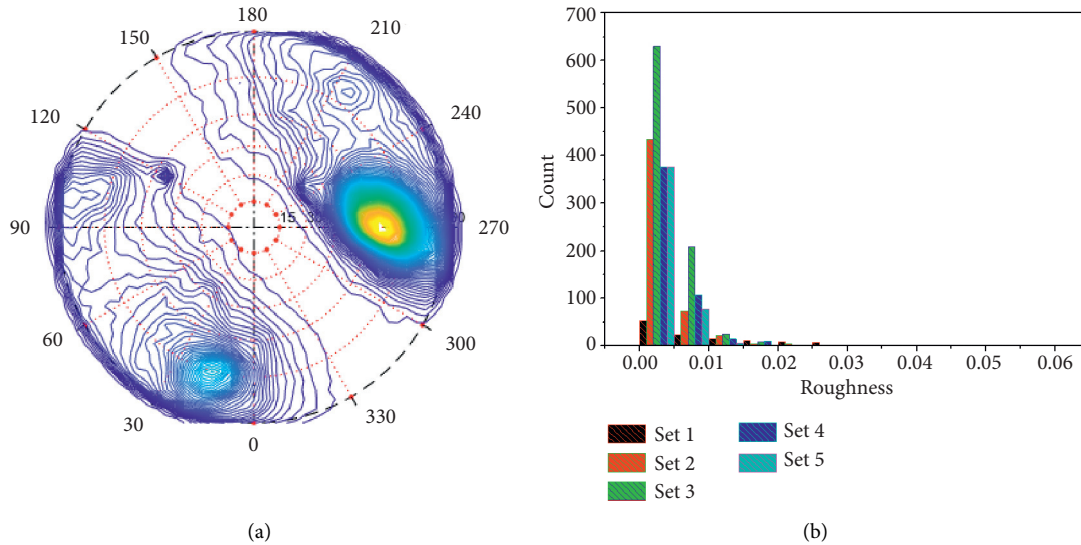


(a)

(b)

FIGURE 10: The extracted discontinuities information.

of dip and dip direction: set1: $217°∠20°$, set2: $277°∠40°$, set3: $277°∠40°$, sset4: $100°∠15°$, and set5: $120°∠50°$. As there is no triangulation and resampling for the point cloud in the calculation process, we can extract the roughness of discontinuities. In this paper, the roughness of discontinuities is defined as the average distance between the point cloud of the same discontinuity and the fitting plane. As shown in Figure 10(b), it can be seen that the roughness is less than 1 cm for most discontinuities, and only a few have a roughness of more than 2 cm.

## 6. Discussion

In the TSL point cloud, the density of points is anisotropic and inhomogeneous so that the hyperparameters *MinPts* and $\epsilon$ in the DBSCSAN algorithm can hardly be determined reasonably. Consequently, we proposed a dynamic DBSCAN algorithm, which only needs one

hyperparameter. During this study, the effectiveness and accuracy of the dynamic DBSCAN algorithm are compromised by several factors. The influence of these factors was studied by model test. When the roughness of the structural plane is less than 5 mm, and the included angle is $170°$ or less, the discontinuities could be segmented. However, when the structural plane's roughness reaches 5 mm, the angle between the discontinuities needs to be less than $150°$ to realize the segmentation. Meanwhile, due to the increase of roughness, when the angle between the two discontinuities is $30°$ or less, the point clouds of the two discontinuities are too close to the dividing line, so the segmentation tends to fail.

The computation efficiency and accuracy of the dynamic DBSCAN algorithm are acceptable for practical usage but still need improvement. For case B, when gravel piles are between two discontinuities, it is easy to cause wrong structural plane segmentation. The point cloud classification takes a lot of

computing time because it needs multiple cycles to extract the features of point clouds at different scales.

## 7. Conclusions

This paper proposed a novel algorithm for automatic discontinuity information extraction from a point cloud. The proposed method consists of three steps: (1) through the Random Forest (RF) algorithm, the point cloud is classified automatically, and the point cloud is divided into plane points and boundary points. (2) The dynamic DBSCAN algorithm segments the point cloud data between different discontinuities. (3) The plane fitting of the same structural plane is carried out by the RANSAC algorithm. The dip, dip direction, and roughness of the structural discontinuity are calculated. The process could be carried out without manual intervention and shows good robustness to the roughness and unevenness of rock mass surface. Through the physical model, the application showed great adaptability and accuracy. Consequently, the method could meet realistic engineering needs.

Future research could be focused on the following aspects to improve the method: (1) Through matrix calculation, a large number of cyclic calculations in the algorithm is avoided, and the multiscale spatial features of the point cloud are extracted quickly; (2) automatic interference removal of debris pile to improve the signal to noise ratio of point cloud data. [14–17].

## Data Availability

The datasets are available at http://www.3D-landslide.com/projects/discontinuity/.

## Conflicts of Interest

The authors declare that there are no conflicts of interest.

## Acknowledgments

## References

[1] R. Roncella, G. Forlani, and F. Remondino, "Photogrammetry for geological applications: automatic retrieval of discontinuity orientation in rock slope," in *Electronic Imaging 2005*, pp. 17–27, International Society for Optics and Photonics, 2005.

[2] M. Sturzenegger and D. Stead, "Close-range terrestrial digital photogrammetry and terrestrial laser scanning for discontinuity characterization on rock cuts," *Engineering Geology*, vol. 106, no. 3-4, pp. 163–182, 2009.

[3] D. Tannant, "Review of photogrammetry-based techniques for characterization and hazard assessment of rock faces," *International journal of geohazards and environment*, vol. 1, no. 2, pp. 76–87, 2015.

[4] X. Li, J. Chen, and H. Zhu, "A new method for automated discontinuity trace mapping on rock mass 3D surface model," *Computers & Geosciences*, vol. 89, pp. 118–131, 2016.

[5] G. Gigli and N. Casagli, "Semi-automatic extraction of rock mass structural data from high resolution LIDAR point clouds," *International Journal of Rock Mechanics and Mining Sciences*, vol. 48, no. 2, pp. 187–198, 2011.

[6] P. Assali, P. Grussenmeyer, T. Villemin, N. Pollet, and F. Viguier, "Surveying and modeling of rock discontinuities by terrestrial laser scanning and photogrammetry: semi-automatic approaches for linear outcrop inspection," *Journal of Structural Geology*, vol. 66, pp. 102–114, 2014.

[7] J. Chen, H. Zhu, and X. Li, "Automatic extraction of discontinuity orientation from rock mass surface 3D point cloud," *Computers & Geosciences*, vol. 95, pp. 18–31, 2016.

[8] S. Chen, M. L. Walske, and I. J. Davies, "Rapid mapping and analysing rock mass discontinuities with 3D terrestrial laser scanning in the underground excavation," *International Journal of Rock Mechanics and Mining Sciences*, vol. 110, pp. 28–35, 2018.

[9] M. O. Idrees and B. Pradhan, "Geostructural stability assessment of cave using rock surface discontinuity extracted from terrestrial laser scanning point cloud," *Journal of Rock Mechanics and Geotechnical Engineering*, vol. 10, no. 3, pp. 534–544, 2018.

[10] X. Li, Z. Chen, J. Chen, and H. Zhu, "Automatic characterization of rock mass discontinuities using 3D point clouds," *Engineering Geology*, vol. 259, Article ID 105131, 2019.

[11] J. J. Monsalve, J. Baggett, R. Bishop, and N. Ripepi, "Application of laser scanning for rock mass characterization and discrete fracture network generation in an underground limestone mine," *International Journal of Mining Science and Technology*, vol. 29, no. 1, pp. 131–137, 2019.

[12] L. Torre-Toaj, A. Bastarrika, A. Boyano, J. M Lopez Guede, and M Grana, "Above-ground biomass estimation from Li-DAR data using random forest algorithms," *Journal of Computational Science*, vol. 58, Article ID 101517, 2022.

[13] H. Chen, M. Liang, and W. Liu, "An approach to boundary detection for 3D point clouds based on DBSCAN clustering," *Pattern Recognition*, vol. 124, Article ID 108431, 2022.

[14] N. Barton, R. Lien, and J. Lunde, "Engineering classification of rock masses for the design of tunnel support," *Rock Mechanics Felsmechanik Mcanique des Roches*, vol. 6, no. 4, pp. 189–236, 1974.

[15] Isrm, "Suggested methods for the quantitative description of discontinuities in rock masses," *International Journal of Rock Mechanics and Mining Science & Geomechanics Abstracts*, vol. 15, pp. 319–368, 1978.

[16] J. A. Franklin, N. H. Maerz, and C. P. Bennett, "Rock mass characterization using photoanalysis," *International Journal of Mining and Geological Engineering*, vol. 6, no. 2, pp. 97–112, 1988.

[17] S. D. Priest, *Discontinuity Analysis for Rock Engineering*, Chapman & Hall, London, UK, 1993.